Journal of Systems Engineering and Electronics
Vol. 33, No. 3, June 2022, pp.585 – 593

An interference suppression algorithm for cognitive bistatic airborne radars

XIA Deping[1,2,*], ZHANG Liang[1,2], WU Tao[2], and HU Wenjun[2]

1. National Laboratory of Radar Signal Processing, Xidian University, Xi'an 710071, China;
2. Nanjing Research Institute of Electronics Technology, Nanjing 210039, China

Abstract: Interference suppression is a challenge for radar researchers, especially when mainlobe and sidelobe interference coexist. We present a comprehensive anti-interference approach based on a cognitive bistatic airborne radar. The risk of interception is reduced by lowering the launch energy of the radar transmitting terminal in the direction of interference; main lobe and sidelobe interferences are suppressed via cooperation between the two radars. The interference received by a single radar is extracted from the overall radar signal using multiple signal classification (MUSIC), and the interference is cross-located using two different azimuthal angles. Neural networks allowing good, non-linear non-parametric approximations are used to predict the location of interference, and this information is then used to preset the transmitting notch antenna to reduce the likelihood of interception. To simultaneously suppress mainlobe and sidelobe interferences, a blocking matrix is used to mask mainlobe interference based on azimuthal information, and an adaptive process is used to suppress sidelobe interference. Mainlobe interference is eliminated using the data received by the two radars. Simulation verifies the performance of the model.

Keywords: interference suppression, cognitive bistatic airborne radar, neural network, blocking matrix.

DOI: 10.23919/JSEE.2022.000056

1. Introduction

Bistatic radar airborne systems are being increasingly used because they are not susceptible to interference. As clutter is range dependent, the geometry of bistatic radars is more complicated than that of monostatic radars. Clutter mitigation has been extensively studied [1−5]; space-time adaptive processing (STAP) effectively reduces clutter, and several techniques have been developed to deal with the clutter range dependence of bistatic radar, which include angle-Doppler compensation (ADC) [6], Doppler warping [7], space-time interpolation [8], and derivative-based updating (DBU) [9]. Knowledge-aided STAP methods [10,11] can also be used to ensure range-dependent clutter suppression. Sparse recovery algorithms have been applied to STAP to reduce the number of training samples needed. Compared to the conventional STAP algorithm, the sparse recovery algorithm accurately estimates the clutter spectrum using fewer training samples [12,13].

Suppression of mainlobe interference is another important function of a bistatic radar. Saini et al. [14] proposed a new method of direct path interference suppression based on dynamic compensation. In [15,16], a multi-station radar system was used to exploit different spatial fluctuation characteristics of the target echo and interference to suppress mainlobe interference. Another mainlobe interference suppression algorithm based on the amplitude ratio was proposed in [17]. Thus, although mainlobe interference suppression is often addressed, simultaneous suppression of both mainlobe and sidelobe interferences has received little attention. When complex, electromagnetic interference countermeasures are in force, a wide-field areal radar system is often subject to simultaneous mainlobe and sidelobe interferences, and sources of unintentional interference may change within a few seconds. Rapid determination of the interference location is needed, along with suppression of the interference and presetting of the transmitting notch antenna. Cognitive radar systems [18] involve continuous and intelligent interactions among the transmitter, the receiver, and the environment; the information received (in the form of radar returns) is memorized. Cognitive radar is well-suited to environments with non-stationary interference sources in which the next interference location must be predicted.

In this study, a neural network is used to create a cognitive bistatic airborne radar, to identify the location of interference, to preset the transmitting notch antenna and suppress mainlobe and sidelobe interferences. It is assumed that the system is aware of signal sources that

Manuscript received March 17, 2021.
*Corresponding author.

may act as interference. A bistatic radar not only estimates the direction of the interference, but also predicts its next possible location. When a bistatic radar is switched on, its two beams simultaneously align with the interference, and the transmitted interference data reveal the location of the interference. The transmitting notch antenna is preset in the predicted direction of interference, and the data received by the two radars are simultaneously processed to cancel interference. Mainlobe interference can be suppressed by direct cancellation; however, as mainlobe and sidelobe interferences often coexist, the residual interference remains relatively large and the received response beam is thus distorted. We develop a cascaded interference cancellation architecture based on a cognitive bistatic airborne radar. First, the mainlobe interference of a single radar is screened by a blocking matrix on the basis of the direction of interference, and the sidelobe interference is then suppressed by adaptive processing; finally, the mainlobe interference is suppressed by cancelling the data received from the two radars.

To improve the accuracy of interference localization, we use passive and active detection methods. Interference prediction by a neural network does not require active detection, which saves time. To demonstrate the utility of the cognitive radar, we describe interference cancellation by a T/R-R bistatic radar; clutter suppression is not addressed. Sections 2–4 of this paper present model, the interference suppression algorithm, simulations, and conclusions respectively.

2. System introduction

A functional block diagram of the cognitive bistatic radar system is shown in Fig. 1. The system includes two radars. One serves as the primary radar which transmits and receives signals; the other serves as an auxiliary radar which only receives signals. Both radars are capable of active and passive detection. The source of interference is predicted by a neural network. The two radars are synchronized in terms of data transmission via broadband links. The red pentagram in Fig. 1 indicates the source of interference.

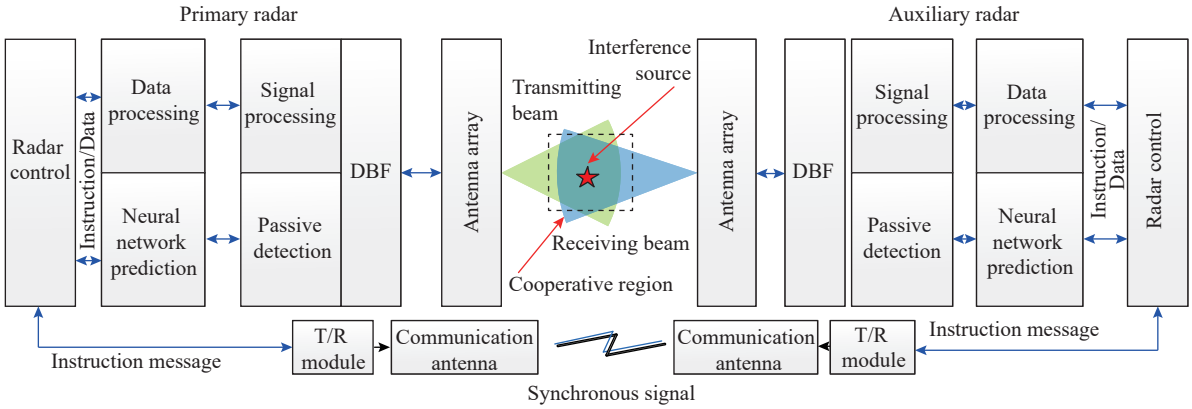

Fig. 1 Block diagram of a cognitive bistatic airborne radar

The cognitive bistatic radar operates in the passive detection mode; the two radars receive interference via N channels and engage in passive detection. The direction of the interference is estimated using the multiple signal classification (MUSIC) algorithm, and locational information is obtained via a cross-sectional approach using two different azimuthal angles. This information is transferred to a neural network; interference locations are newly predicted based on historical information and fed back to the control, which directs the beams of the two radars. Then, mainlobe and sidelobe interferences are suppressed and the risk of interception reduced. This interference mitigation enhances the signal to interference plus noise ratio (SINR) of the system. When a bistatic airborne radar is in operation, the receiving modules sample the interference, and transfer the sampled data to the DBF via optical fibers, thus creating N subarray data.

3. Interference suppression algorithm

This section describes our cascaded interference cancellation architecture applied to a cognitive bistatic airborne radar. First, angle and location information is predicted by the neural network. Based on these predictions, the transmitting notch antenna is preset and a block matrix preprocesses the received data, masking mainlobe interference and reducing the impact of the adaptive response on the targets. Single radar-received data are subjected to adaptive processing. Finally, the data received by the two radars are subtracted; mainlobe interference is suppressed and the target is preserved. This cooperative anti-interference bistatic process is explained in Fig. 2.

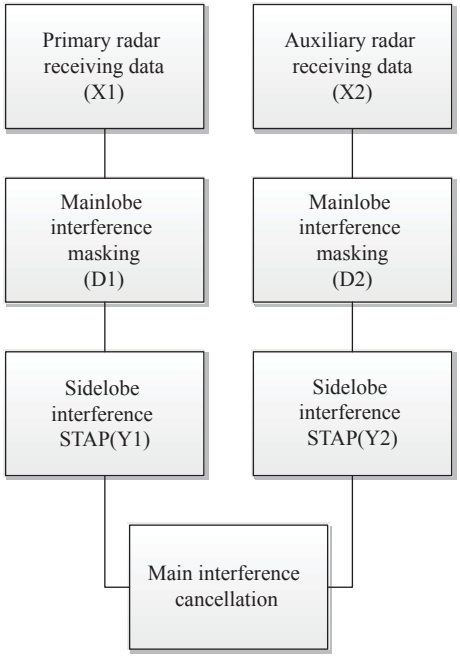

Fig. 2 Cooperative anti-interference process

3.1 Interference confirmation and prediction

3.1.1 Confirmation of the interference location

The MUSIC algorithm rapidly resolves multiple signals using a super-resolution direction of arrival (DOA) estimation technique, and has often been used to derive arrival angles [19]. The radar receiver array consists of N fully digital channels forming N subarray data points. When I narrowband interference signals from the far field $\theta_1,\theta_2,\cdots,\theta_I$ direction are incident on the array, the output data vector is

$$\boldsymbol{X}(t) = \boldsymbol{A}\boldsymbol{s}(t) + \boldsymbol{n}(t) \tag{1}$$

where $\boldsymbol{X}(t) = [x_1(t), x_2(t), \cdots, x_N(t)]^{\mathrm{T}}$ and $\boldsymbol{s}(t) = [s_1(t), s_2(t), \cdots, s_I(t)]^{\mathrm{T}}$ are the received signal vector consisting of I complex envelopes of the uncorrelated signal sources. $\boldsymbol{n}(t) = [n_1(t), n_2(t), \cdots, n_N(t)]^{\mathrm{T}}$ is the N-dimensional white noise vector. $\boldsymbol{A} = [\boldsymbol{a}(\theta_1), \boldsymbol{a}(\theta_2), \cdots, \boldsymbol{a}(\theta_I)]^{\mathrm{T}}$ is the steering vector matrix; $\boldsymbol{a}(\theta_i) = [1, \mathrm{e}^{-\mathrm{j}\mu_i}, \cdots, \mathrm{e}^{-\mathrm{j}\mu_i}]^{\mathrm{T}}$, where $\mu = 2\pi/\lambda d\sin\theta$, λ is the operating wavelength, d is the interelement spacing, and i is the interference number.

The output covariance matrix is

$$\boldsymbol{R} = \mathrm{E}\{\boldsymbol{X}(t)\boldsymbol{X}^{\mathrm{H}}(t)\} = \boldsymbol{A}\boldsymbol{P}\boldsymbol{A}^{\mathrm{H}} + \sigma_n^2\boldsymbol{I}_M \tag{2}$$

where $\mathrm{E}\{\cdot\}$ is the mathematical expectation, σ_n^2 is the sensor noise power, $\boldsymbol{I}_M$ is an M-order identity matrix, and $\boldsymbol{P} = \mathrm{E}\{\boldsymbol{s}(t)\boldsymbol{s}^{\mathrm{H}}(t)\}$ is the signal covariance matrix.

The eigenstructure decomposition of $\boldsymbol{R}$ is

$$\boldsymbol{R} = \sum_{i=1}^{M} \alpha_i \boldsymbol{u}_i \boldsymbol{u}_i^{\mathrm{H}} = \boldsymbol{S}\boldsymbol{\Lambda}\boldsymbol{S}^{\mathrm{H}} + \sigma_n^2\boldsymbol{G}\boldsymbol{G}^{\mathrm{H}} \tag{3}$$

where $\boldsymbol{S} = [u_1, u_2, \cdots, u_D]$ is the signal subspace, $\boldsymbol{G} = [u_{D+1}, u_{D+2}, \cdots, u_M]$ is the noise subspace, $\boldsymbol{\Lambda} = \mathrm{diag}\{\alpha_1, \alpha_2, \cdots, \alpha_D\}$ is a diagonal matrix, and $\alpha_1 \geqslant \alpha_2 \geqslant \cdots \geqslant \alpha_D > \alpha_{D+1} = \cdots = \alpha_M = \sigma_n^2$. Thus, by determining the steering vectors orthogonal to the eigenvectors associated with the eigenvalues of $\boldsymbol{R}$, the DOA can be calculated as

$$f(\theta) = \frac{1}{\boldsymbol{a}^{\mathrm{H}}(\theta)\boldsymbol{G}\boldsymbol{G}^{\mathrm{H}}\boldsymbol{a}(\theta)}. \tag{4}$$

A schematic of the cross-location is shown in Fig. 3. An (x, y) coordinate system is constructed, assuming that the speed and location of the airborne radar are compensated. In this system, the primary radar is located at (0,0) and its velocity vector is assumed to be horizontal. And the angle between the primary radar and the interference is α with respect to the x-axis. The auxiliary radar is located at (L,0), its velocity is assumed to be both horizontal, and the angle between the auxiliary radar and interference is β with respect to the x-axis. L is the baseline length of the two radars. Point I indicates the interference position, and the position (x_0, y_0) is calculated as

$$\begin{cases} x_0 = \dfrac{L\cos\alpha\sin\beta}{\sin(\beta-\alpha)} \\ y_0 = \dfrac{L\sin\alpha\sin\beta}{\sin(\beta-\alpha)} \end{cases}. \tag{5}$$

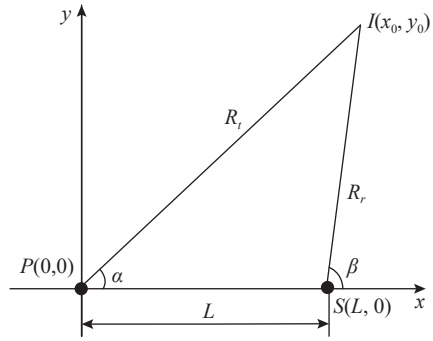

Fig. 3 Schematic of the cross-location

R_t is the distance between the interference and the primary radar, and R_r is that between the interference and the auxiliary radar; they are yielded by the triangle relationship.

3.1.2 Prediction of interference location

To preset the zero point of the transmitting antenna and construct a blocking matrix that masks mainlobe interference, it is necessary to derive the angle and position of the interference.

A Kalman filter based on the previous state sequence of the system is optimal for estimating that state [20,21]. The prediction is unbiased and stable. A Kalman filter is

linearly recursive. It includes state and observation equations; the equation of state is

$$\boldsymbol{x}_k = \boldsymbol{F}\boldsymbol{x}_{k-1} + \boldsymbol{B}\boldsymbol{u}_k + \boldsymbol{w}_k, \tag{6}$$

and the equation of observation is

$$\boldsymbol{y}_k = \boldsymbol{H}\boldsymbol{x}_k + \boldsymbol{v}_k, \tag{7}$$

where $\boldsymbol{x}_k, \boldsymbol{x}_{k-1}$ are the state vectors of the system at k and $k-1$, respectively; $\boldsymbol{F}$ is the state transition matrix from $k-1$ to k; $\boldsymbol{B}$ is the system control action matrix; $\boldsymbol{u}_k$ is the deterministic input of the system; $\boldsymbol{H}$ is the measurement matrix; $\boldsymbol{y}_k$ is the state observation vector at time k; $\boldsymbol{w}_k$ is the process noise; and $\boldsymbol{v}_k$ is the measurement noise. $\boldsymbol{w}_k$ and $\boldsymbol{v}_k$ are mutually independent.

The hypothetical system state vector is

$$\boldsymbol{x}_k = [\boldsymbol{x}_{Lx}, \boldsymbol{x}_{Ly}, \boldsymbol{x}_{pa}, \boldsymbol{x}_{aa}] \tag{8}$$

where $\boldsymbol{x}_{Lx}, \boldsymbol{x}_{Ly}$ represent the positions of the interference on the x- and y-axes, respectively; $\boldsymbol{x}_{pa}, \boldsymbol{x}_{aa}$ are the angles between the primary and auxiliary radars, and interference with respect to the x-axis, respectively. The steps for Kalman prediction are shown as follows:

$$\boldsymbol{x}_{k,k-1} = \boldsymbol{F}\boldsymbol{x}_{k-1} + \boldsymbol{B}\boldsymbol{u}_k, \tag{9}$$

$$\boldsymbol{P}_{k,k-1} = \boldsymbol{F}\boldsymbol{P}_{k-1}\boldsymbol{F}^{\mathrm{T}} + \boldsymbol{Q}, \tag{10}$$

$$\boldsymbol{K}_k = \boldsymbol{P}_{k,k-1}\boldsymbol{H}^{\mathrm{T}}\left(\boldsymbol{H}\boldsymbol{P}_{k,k-1}\boldsymbol{H}^{\mathrm{T}} + \boldsymbol{R}\right)^{-1}, \tag{11}$$

$$\boldsymbol{x}_k = \boldsymbol{x}_{k,k-1} + \boldsymbol{K}_k[\boldsymbol{y}_k - \boldsymbol{H}\boldsymbol{x}_{k,k-1}], \tag{12}$$

$$\boldsymbol{P}_k = (\boldsymbol{I} - \boldsymbol{K}_k\boldsymbol{H})\boldsymbol{P}_{k,k-1}, \tag{13}$$

where $\boldsymbol{Q}$, $\boldsymbol{R}$, $\boldsymbol{K}$, and $\boldsymbol{P}$ are the input variance, measurement variance, Kalman gain, and prediction variance, respectively. $\boldsymbol{x}_{k,k-1}$ is the predicted value and $\boldsymbol{x}_k$ is the correction of $\boldsymbol{x}_{k,k-1}$. $\boldsymbol{P}_{k,k-1}$ is the covariance matrix of $\boldsymbol{x}_{k,k-1}$ and $\boldsymbol{P}_k$ is the covariance matrix of $\boldsymbol{x}_k$.

As the calculation error of a Kalman filter is relatively large, divergence is common over time, especially when the features of the interference change. Both the interference angle and position are prone to bias, which affects block matrix construction. Therefore, a neural network is used to improve the accuracy of interference estimation. A non-linear non-parametric approach is used to accurately approximate any continuous function [22]; this is easier to apply and more accurate than any other predictive technique when the functional relationship between the independent and dependent variables is unknown [23]. Initially, consecutive interference locations are identified and arranged in a "triangle" (a time series sequence). This is input to neural networks that optimally adjust the weights and self-trains for optimal fitting, until the performance criterion is met.

Here, we use a generalized regression neural network (GRNN) [24], which includes input, pattern, summation, and output layers. The model architecture and operation are shown in Fig. 4.

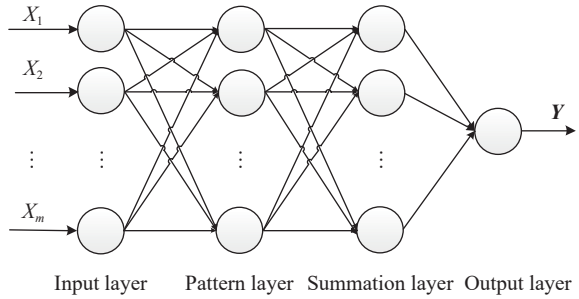

Fig. 4 Architecture of the GRNN model

The following equation summarizes the GRNN logic using an equivalent nonlinear regression formula

$$\mathrm{E}[\boldsymbol{Y}/\boldsymbol{X}] = \frac{\int_{-\infty}^{\infty} \boldsymbol{Y} f(\boldsymbol{X}, \boldsymbol{Y})\,\mathrm{d}\boldsymbol{Y})}{\int_{-\infty}^{\infty} f(\boldsymbol{X}, \boldsymbol{Y})\,\mathrm{d}\boldsymbol{Y})} \tag{14}$$

where $\boldsymbol{X}$ is the input vector $(X_1, X_2, \cdots, X_m)$ consisting of m predictor variables, and $\boldsymbol{Y}$ is the output predicted by the GRNN. E[$\boldsymbol{Y}$/$\boldsymbol{X}$] is the expected value of output $\boldsymbol{Y}$ given input vector $\boldsymbol{X}$, and $f(\boldsymbol{X},\boldsymbol{Y})$ is the joint probability density of $\boldsymbol{X}$ and $\boldsymbol{Y}$ [25]. The model can be expressed as an $M-1$ GRNN model, thus with an M-dimensional input and a one dimensional output. An optimal GRNN model is obtained via three steps. First, the original data are divided into two parts; the two most recent datasets are used for testing, and the rest for training. To minimize the network root mean square error (RMSE), the training set is smoothed using M values to identify the best smoothing factor. Then, the final M values of the original data are used as inputs to predict future data.

A schematic of interference location prediction is shown in Fig. 5. The coordinate system is shown in Fig. 3. Point P' indicates the primary radar location at the time of prediction; the velocity is assumed to be horizontal, and the angle between the primary radar and interference is α' with respect to the x-axis. Point S' is the auxiliary radar location at the time of prediction; the velocity is assumed to be horizontal, and the angle between the auxiliary radar and interference is β' with respect to the x-axis. R_t' is the distance between the predicted interference position and the primary radar, and R_r' is the distance between the predicted interference position and the auxiliary radar. L' is the distance between the predicted primary radar position and the predicted auxiliary radar position.

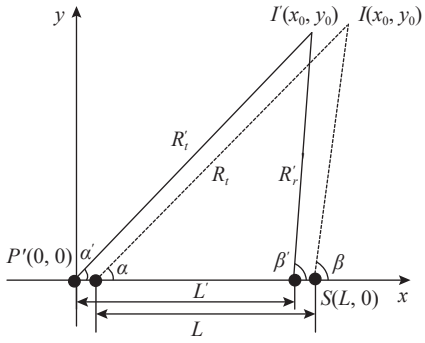

Fig. 5 Schematic of location prediction

Point I' is the predicted interference position, and its angle with respect to the x-axis can be calculated as

$$\begin{cases} \alpha' = \arcsin \dfrac{x_0'}{\sqrt{x_0'^2 + y_0'^2}} \\ \beta' = \arcsin \dfrac{y_0'}{\sqrt{(x_0' - L')^2 + y_0'^2}} \end{cases}. \tag{15}$$

3.2 Presetting the transmitting pattern notch and interference cancellation

In general, the transmission pattern is

$$F(\theta,\beta) = \sum_{m=0}^{M-1} \sum_{n=0}^{N-1} w_i \mathrm{e}^{\mathrm{j}\frac{2\pi}{\lambda} d(m\sin\theta\cos\beta + n\sin\beta)} \tag{16}$$

where M is the number of antenna rows, N is the number of antenna columns, w_i is the weight of the antenna array element (the transmit weight vector, which is commonly invariant), θ is the azimuth scanning angle, and β is the elevation scanning angle (here β=0). If the direction of interference is known, the transmit weight vector may be modified by presetting the notch in the direction of interference.

Mainlobe interference is suppressed using data received by the bistatic radar. It is possible to directly subtract the data received by the two radars, and then further suppress interference via adaptive processing. However, to effectively restrain interference, the distance between the two radar stations must be appropriate for target echo decorrelation, calculated as

$$D > R\frac{\lambda}{2S} \tag{17}$$

where D is the distance between the two radars, R is the distance between the target relative to the primary and auxiliary radars, and S is the cross-sectional target size. This is also a basic requirement for mainlobe cancellation by the two radars. In practice, many signals are mixed and direct data cancellation will restrain surplus interference. Thus, we develop a cascaded interference cancellation architecture.

First, the blocking matrix is used to mask the mainlobe interference experienced by the primary and auxiliary radars, based on the prior direction, and to overcome the need to calculate the covariance matrix. When the received data are preprocessed by the blocking matrix, we obtain the output

$$\boldsymbol{D} = \boldsymbol{B}_I \boldsymbol{X} \tag{18}$$

where $\boldsymbol{B}_I$ is the blocking matrix. Below, we use a mainlobe interference as an example when setting the blocking matrix, and $\boldsymbol{B}_I$ can be expressed as

$$\boldsymbol{B}_I = \begin{bmatrix} 1 & -\mathrm{e}^{\mathrm{j}\mu_1} & 0 & \cdots & 0 & 0 \\ 0 & 1 & -\mathrm{e}^{\mathrm{j}\mu_1} & \cdots & 0 & 0 \\ \vdots & \vdots & \ddots & \ddots & \vdots & \vdots \\ 0 & 0 & \cdots & 1 & -\mathrm{e}^{\mathrm{j}\mu_1} & 0 \\ 0 & 0 & \cdots & 0 & 1 & -\mathrm{e}^{\mathrm{j}\mu_1} \end{bmatrix}_{(N-1)\times N} \tag{19}$$

where $\mu_1 = 2\pi/\lambda d \sin\theta_1$, θ_1 is the direction of mainlobe interference. Equation (19) is substituted into (18) to give

$$\boldsymbol{D} = \begin{bmatrix} 1 & -\mathrm{e}^{\mathrm{j}\mu_1} & 0 & \cdots & 0 & 0 \\ 0 & 1 & -\mathrm{e}^{\mathrm{j}\mu_1} & \cdots & 0 & 0 \\ \vdots & \vdots & \ddots & \ddots & \vdots & \vdots \\ 0 & 0 & \cdots & 1 & -\mathrm{e}^{\mathrm{j}\mu_1} & 0 \\ 0 & 0 & \cdots & 0 & 1 & -\mathrm{e}^{\mathrm{j}\mu_1} \end{bmatrix} \cdot \begin{bmatrix} x_1(t) \\ x_2(t) \\ \vdots \\ x_N(t) \end{bmatrix} = \begin{bmatrix} x_1(t) - \mathrm{e}^{\mathrm{j}\mu_1} x_2(t) \\ x_2(t) - \mathrm{e}^{\mathrm{j}\mu_1} x_3(t) \\ \vdots \\ x_{N-1}(t) - \mathrm{e}^{\mathrm{j}\mu_1} x_N(t) \end{bmatrix}. \tag{20}$$

In (20), the dimension of the blocking matrix is $(N-1) \times N$. Therefore, a signal pre-processed by this matrix lacks one dimension. The physical explanation is that the next path is weighted, and the current path is then canceled; one degree of freedom is lost. When constructing the blocking matrix, it is critical that the interference angle is correct. If the estimation of angle is biased, interference suppression is compromised, which explains why a GRNN is used herein for interference estimation.

The blocking matrix method can be used to suppress mainlobe interference encountered by a monostatic radar, but it is accompanied by high sidelobe and mainbeam distortion. When the target signal and mainlobe interference enter from the same direction, the matrix suppresses both the interference and signal, rendering it impossible to detect the target [26,27].

Next, sidelobe interference suppression of the primary and auxiliary radars is performed. By weighting the output data $\boldsymbol{D}$ using certain criteria, we derive the output as follows:

$$\boldsymbol{y} = \boldsymbol{W}^{\mathrm{H}} \boldsymbol{D} \tag{21}$$

where $\boldsymbol{W}$ is the adaptive weight vector. The same algorithm is used for both radars; the subscript is thus omitted here.

According to the least-squares criterion, the optimal weight is

$$w_{\text{opt}} = \frac{\boldsymbol{R}^{-1}\boldsymbol{S}}{\boldsymbol{S}^{\text{H}}\boldsymbol{R}^{-1}\boldsymbol{S}} \tag{22}$$

where $\boldsymbol{R}$ is the covariance matrix and $\boldsymbol{S}$ is the space-time joint steering vector, defined as

$$\boldsymbol{S} = \boldsymbol{S}_s \otimes \boldsymbol{S}_t \tag{23}$$

where $\boldsymbol{S}_s = [1, \exp(\text{j}\omega_s), \cdots, \exp(\text{j}(N-1)\omega_s)]$ is the spatial steering vector, ω_s is the normalized frequency of space, $\boldsymbol{S}_t = [1, \exp(\text{j}\omega_t), \cdots, \exp(\text{j}(\text{k}-1)\omega_t)]$ is the temporal steering vector, and ω_t is the normalized Doppler frequency.

Finally, depending on the phase, and the time and beam synchronization of the bistatic radar, the bistatic received data can be canceled using the following formula:

$$\boldsymbol{Y} = w_{\text{opt1}}\boldsymbol{X}_1 - g w_{\text{opt2}}\boldsymbol{X}_2 \tag{24}$$

where $\boldsymbol{X}_1$ and w_{opt1} are the primary radar-received data and the optimal weight; $\boldsymbol{X}_2$ and w_{opt2} are the auxiliary radar-received data and optimal weight; and g is the optimization coefficient for the two datasets. The angle between the two radars and the interference are both adequately large, and correlate with the target echo.

4. Simulation

We present a simulation that demonstrates the superior performance afforded by neural networks. The principal parameters of a bistatic radar are listed in Table 1. The additional parameters are as follows: side-looking arrays with no platform crab, velocity of 135 m/s, aircraft heights of 7 500 m, and baseline length of 200 km. The direction of the desired signal is set at the 100th sampling point toward 1.6º. The signal to noise ratio (SNR) is 30 dB, the angles of the interfering signals are 1.6º and −45º, and their respective interference to noise ratios (INRs) are 35 dB and 45 dB. The interfering signal constitutes mainlobe interference at 1.6º and exhibits the same angle as the desired signal. All angle and sampling point parameters refer to the one radar, because the algorithm used by the other radar is similar. There is no need to list the parameters separately.

Table 1 Bistatic airborne radar specifications

Radar	Specification	Value
Primary radar	Carrier frequency/GHz	1.25
	Pulse repetition frequency/Hz	2 000−8 000
	Pulse width/μs	12−100
	Peak output power/kW	100
	Transmitter number	48
	Receiver number	48
	Signal bandwidth/MHz	5
	Beamwidth/(º)	2.9
	Sampling interval/s	1
	Polarization	Horizontal
Auxiliary radar	Carrier frequency/GHz	1.25
	IF bandwidth/MHz	60
	IF sample frequency/MHz	200
	Receiver number	48
	Beamwidth/(º)	3.4
	Polarization	Horizontal

Fig. 6 depicts the assumed trajectory of the mainlobe interference, whose initial position is (200 km, 200 km).

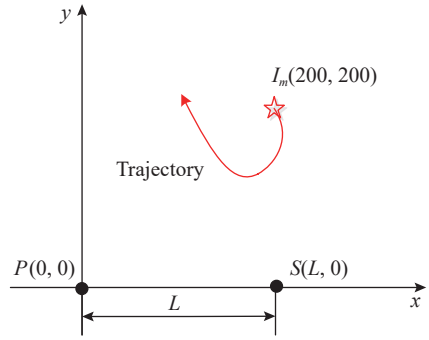

Fig. 6 Assumed trajectory of the mainlobe interference

4.1 Interference confirmation

Based on its initial location, we can estimate the azimuthal angle of the interference. Using the results of Fig. 6, the DOA of the primary radar and the auxiliary radar are shown in Fig. 7(a) and Fig. 7 (b), respectively.

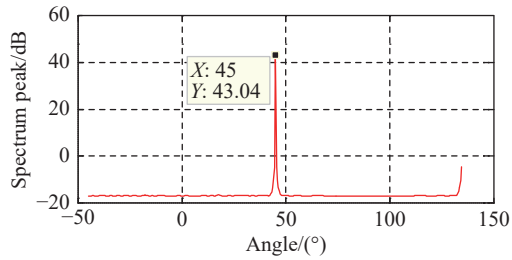

(a) DOA of the primary radar

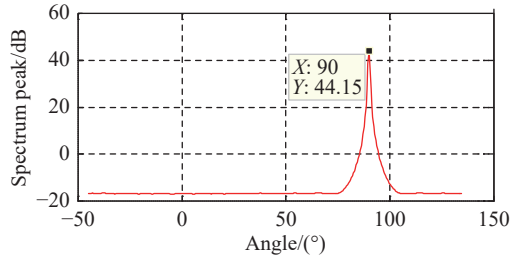

(b) DOA of the auxiliary radar

Fig. 7 DOA values estimated using the MUSIC algorithm

Substituting the two radar DOA results and the baseline into (5), we can estimate the locations (200 km,200 km) of interference. The bistatic radar may receive location information regardless of a change in interference position, but not in real time.

4.2 Interference predictions

The initial interference data are input into the neural networks and the Kalman filter, and the simulations are then performed. The time-series sequences of the successive interference locations are loaded into a GRNN time-series model. The system performance criterion is the RMSE. Predictive plots of the angle time series are shown in Fig. 8(a) and Fig. 8(b). The plots in Fig. 8(c) and Fig. 8(d) show the predicted interference trajectories. Fig. 8(d) is an enlargement of part of Fig. 8(c).

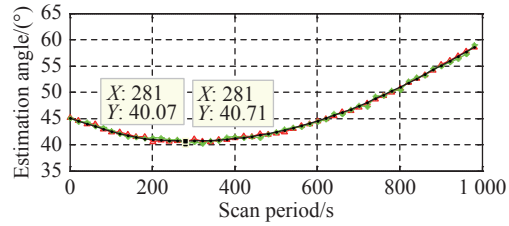

(a) Angle time series prediction for the primary radar

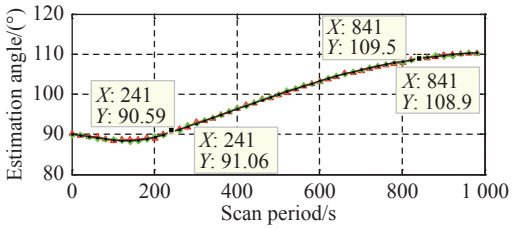

(b) Angle time series prediction for the auxiliary radar

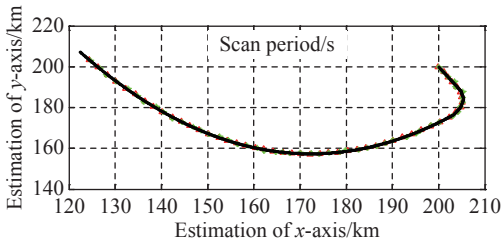

(c) Predicted trajectory of interference

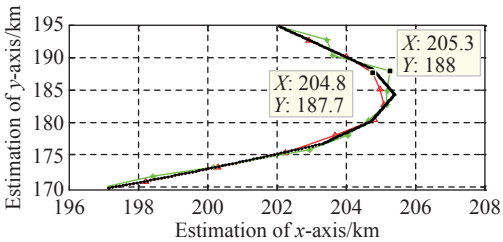

(d) Enlarged view of the predicted trajectory of interference

: GRNN estimation; : Kalman estimation;
: Original data.

Fig. 8 Prediction performance plots

Fig. 8(a) and Fig. 8(b) show that the angle estimation error of the Kalman filter is larger than that of the GRNN. The maximum error is 0.64º, which would affect the construction of the blocking matrix. Similarly, Fig. 8(c) and Fig. 8(d) show that the position estimation error of the Kalman filter is larger than that of the GRNN. The maximum error is 300 m. The performance of the GRNN is obviously superior to that of the Kalman filter.

4.3 Presetting the notch of the transmission pattern

The predicted angles are used to preset the notch of the transmission pattern. Fig. 9 shows the result; the relative gain is plotted against the azimuthal angle. The notch points toward the predicted interference; the zero point is taken to be 20º, which greatly reduces the risk of interception. The angle of elevation is not considered here.

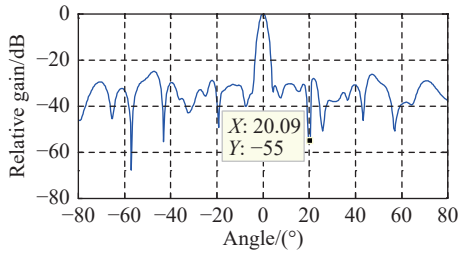

Fig. 9 The zero point transmission pattern

4.4 Simulation of space domain response

Fig. 10(a) shows the space domain response without a blocking matrix; the array gain is plotted against the azimuthal angle. The null depth is found in the direction of interference; one zero point lies at 1.6º and the other at −45º. The mainbeam pattern is distorted, compromising target detection. Fig. 10(b) shows the space domain response after mainlobe interference has been masked. The proposed pattern is very close to quiescent; thus, our method effectively suppresses sidelobe interference while maintaining the mainbeam pattern. The zero point position at −45º lies at the angle of sidelobe interference. Fig. 10(c) shows that, given the angle estimation error of the Kalman filter, the blocking matrix cannot completely mask the mainlobe interference at 1.6º. The residual interference affects the response of the space domain.

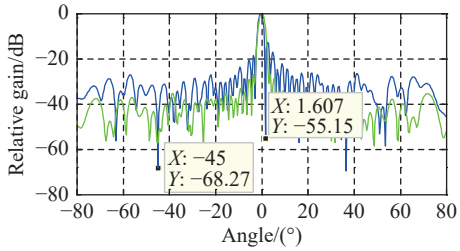

: A mainlobe interference and a sidelobe interference;
: No interference.

(a) Response without a blocking matrix

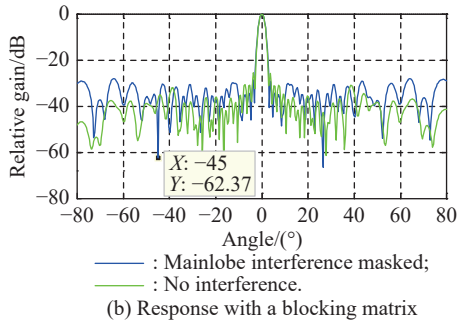

(b) Response with a blocking matrix

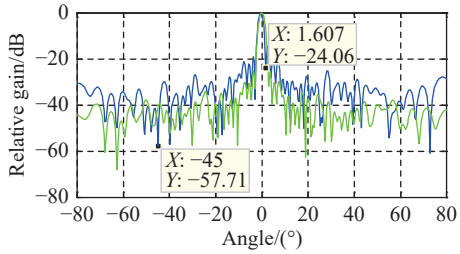

(c) Response with a blocking matrix (showing the effect of the angle estimation error)

Fig. 10 Space domain responses

4.5 Simulation of target detection

To explore the effect of mainlobe interference on the radar function, we test the SINR performance of our method.

Fig. 11 shows the results when the azimuth of the mainlobe interference is within the main beam (from −2.4° to 2.4°). The figure shows that, unlike a monostatic radar encountering mainlobe interference, bistatic cooperative radars can detect a target in the direction of mainlobe interference, eliminating the influence of interference on detection performance over a certain angle.

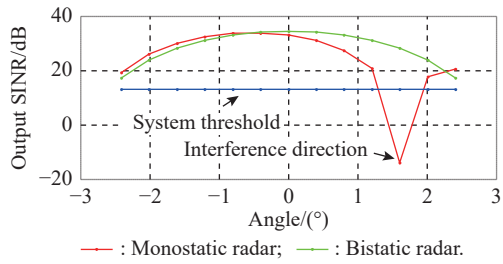

Fig. 11 Performance evaluation: target detection after canceling mainlobe interference

Fig. 12 shows target detection after mainlobe interference is directly subtracted; the output SINR of 28.5 dB reflects an SINR loss of about 8 dB. The mainlobe interference is well-suppressed, but at a high processing cost. When the target SINR is less than this value, target detection is affected and often impossible.

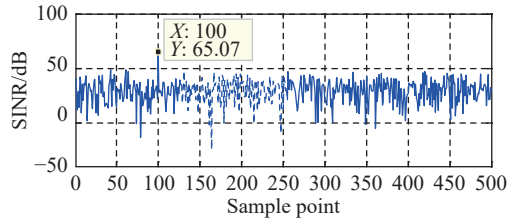

Fig. 12 Output SINR based on the mainlobe interference directly subtracted

Fig. 13 shows target detection after the mainlobe interference is suppressed by the blocking matrix. The output SINR is 34.5 dB and the SINR loss is about 2 dB. Mainlobe interference suppression is greatly improved.

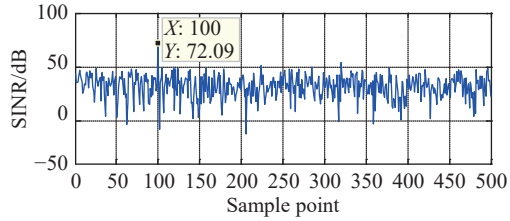

Fig. 13 Output SINR based on the mainlobe interference suppressed by the blocking matrix

5. Conclusions

We develop an effective bistatic radar architecture for addressing interference. As shown by simulations, the MUSIC algorithm provides exact DOA values, and real-time locations predicted by neural networks are helpful for blocking mainlobe interference, adaptive interference cancellation and reducing the risk of interception. The numerical examples show that the locations of interference are effectively predicted, allowing the launch energy to be reduced in the direction of interference. Mainlobe and sidelobe interferences are suppressed without distorting the mainbeam pattern, and clear improvements in the SINR are evident.

References

[1] KLEMM R. Comparison between monostatic and bistatic antenna configuration for STAP. IEEE Trans. on Aerospace and Electronic Systems, 2000, 36(2): 596–608.

[2] MELVIN W, CALLAHAN M, WICKS M. Adaptive cancellation method for geometry induced nonstationary bistatic clutter environments. IEEE Trans. on Aerospace and Electronic Systems, 2007, 43(2): 651–672.

[3] STINCO P. Performance analysis of bistatic radar and optimization methodology in multistatic radar system. Pisa: University of Pisa, 2012.

[4] AHMED A A, IOANNIS P, BENOIT C. Covariance-free non-homogeneity STAP detector in compound Gaussian clutter based on robust statistics. IET Radar, Sonar and Navigation, 2019, 13(12): 2107–2119.

[5] ZHANG W, AN R X, HE N Y, et al. Reduced dimension STAP based on sparse recovery in heterogeneous clutter environments. IEEE Trans. on Aerospace and Electronics

Systems, 2020, 56(1): 785–795.
[6] HIMED B, ZHANG Y, HAJJARI A. STAP with angle-Doppler compensation for bistatic airborne radars. Proc. of the IEEE National Radar Conference, 2002: 311–317.
[7] BORSARI G. Mitigating effects on STAP processing caused by an inclined array. Proc. of the IEEE Radar Conference, 1998: 135–140.
[8] VARADARAJAN V, KROLIK J K. Joint space-time interpolation for distorted linear and bistatic array geometries. IEEE Trans. on Signal Processing, 2006, 56(3): 848–860.
[9] HAYWARD S D. Adaptive beamforming for rapidly moving arrays. Proc. of the CIE International Conference of Radar, 1996: 480–483.
[10] BLUNT S, GERLACH K, RAMASWAMY M. STAP using knowledge-aided covariance estimation and FRACTA algorithm. IEEE Trans. on Aerospace and Electronic Systems, 2006, 42(3): 1043–1057.
[11] CAPRARO C. Implementing digital terrain data in knowledge-aided space-time adaptive processing. IEEE Trans. on Aerospace and Electronic Systems, 2006, 42(3): 1080–1098.
[12] YANG Z C, LI X, WANG H Q, et al. On clutter sparsity analysis in space-time adaptive processing airborne radar. IEEE Geoscience Remote Sensing Letters, 2013, 10(5): 1214–1218.
[13] HAN S D, FAN C Y, HUANG X T. A novel STAP based on spectrum-aided reduced-dimension clutter sparse recovery. IEEE Geoscience and Remote Sensing Letters, 2017, 14(2): 213–217.
[14] SAINI R, CHERNIAKOV M, LEIRE V. Direct path interference suppression in bistatic system: DTV based radar. Proc. of the International Radar Conference, 2003: 309–314.
[15] CHERNYAK V S. Adaptive mainlobe jamming cancellation and target detection in multistatic radar systems. Proc. of the CIE International Conference of Radar, 1996: 297–300.
[16] ZHOU W G, TAN H Y, LI G, et al. Investigation on dual station cancellation of mainlobe jamming suppression technology. Modern Radar, 2018, 40(7): 83–86. (in Chinese)
[17] ZHAO S S, LIU Z W. Main-lobe jamming suppression method in multiple-radar system. Journal of University of Electronic Science and Technology of China, 2020, 49(4): 584–589. (in Chinese)
[18] ZHANG X, CUI C. Range-spread target detecting for cognitive radar based on track-before-detect. International Journal of Electronics, 2014, 101(1): 74–87.
[19] OSMANO M, SFAR I, GHARASALLAH A. The application of high-resolution methods for DOA estimation using a linear antenna array. International Journal of Microwave and Wireless Technologies, 2014, 7(1): 87–94.
[20] KALMAN R E. A new approach to linear filtering and prediction problems. Journal of Fluids Engineering, 1960, 82(1): 35–45.
[21] LI Y, PANG Y, LI Z X, et al. An intelligent tracking technology based on Kalman and mean shift algorithm. Proc. of the 2nd International Conference on Computer Modeling and Simulation, 2010: 107–109.
[22] ISLAM B. Comparison of conventional and modern load forecasting techniques based on artificial intelligence and expert systems. International Joural of Computer Science Issues, 2011, 8: 504–513.
[23] RAJI M A, ATHAPPILLY K. Comparative predictive analysis of neural networks (NNS) nonlinear regression and classification and regression tree (CART) models. Expert Systems with Applications, 2005, 29(1): 65–74.
[24] SPECHT D F. A general regression neural network. IEEE Trans. on Neural Networks, 1991, 2(6): 568–576.
[25] LEUNG M T, CHEN A S, MANCHA R. Making trading decisions for financial-engineered derivatives: a novel ensemble of neural networks using information content. Intelligent Systems in Accounting, Finance & Management. 2009, 16(4): 257–277.
[26] SU B, WANG Y, LI R F, et al. Mainlobe interference cancel ling method via block matrix. Systems Engineering and Electronics, 2005, 27(11): 1830–1832. (in Chinese)
[27] GAO Y, XU J, LONG T. Performance analysis of anti-jamming method via block matrix. Journal of Signal Processing, 2015, 31(10): 1361–1365. (in Chinese)

Biographies

XIA Deping was born in 1977. He received his B.S. degree in electrical engineering from Harbin Engineering University in 2000 and M.S. degree in signal and information processing from Nanjing University of Science and Technology in 2009. He is currently a Ph.D. candidate of National Laboratory of Radar Signal Processing in Xidian University. He is a senior expert of Chinese Electronics Technology Corporation. His research interests include adaptive signal processing and polarization information processing.
E-mail: xiadeping@cetc.com.cn

ZHANG Liang was born in 1966. He received his B.S. degree in electrical engineering from Wuhan University in 1988 and Ph.D degree in National Laboratory of Radar Signal Processing from Xidian University in 2000. Since 2015, he has been a chief scientist of Chinese Electronics Technology Corporation and a adjunct professor at Xidian University. His current research interests include radar system design and signal processing technology.
E-mail: zhangliang@cetc.com.cn

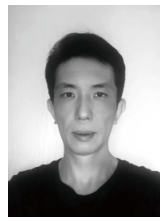

WU Tao was born in 1975. He received his B.E. degree in electrical engineering from Nanjing University of Science and Technology in 1997. He is a senior expert of Chinese Electronics Technology Corporation. He is a senior member of Nanjing Research Institute of Electronic Technology. His research interest is systems engineering of radar.
E-mail: wutao12@cetc.com.cn

HU Wenjun was born in 1984. He received his M.S. degree from Nanjing Research Institute of Electronics Technology, Nanjing, China, in 2008. His major work is communication and information system. He works as a senior engineer currently in Nanjing Research Institute of Electronics Technology. His research interest is radar system design.
E-mail: huwenjun@cetc.com.cn